Monte Carlo Simulations of an Ising Model Ferromagnet with Defects

Mahesh Dhulipala, Matthew Dobson

Department of Mathematics, University of Massachusetts, Amherst, MA 01002 USA

Abstract:
This paper will examine one and two dimensional Ising Models of a ferromagnet. In particular, we will examine the behavior of magnetization as it relates to temperature, external magnetization, and various defects. The results of our simulations are compared to the analytic solutions derived by Ernst Ising and Lars Onsager. In addition we will briefly discuss uncertainty quantification for the homogenous 1D Ising model.

Index Terms: Ising Model, Monte Carlo Simulation.

1. Theory

1.1. Introduction

The Ising Model, first developed by Ernst Ising and Wilhelm Lenz in the 1920s, has played an instrumental role in understanding the behavior of phase transitions in physical materials. The model is best described as a system composed of spins; each spin can either be up$(+)$ or down$(-)$. Figure 1 illustrates a 1D model. When studying the Ising model, we are often concerned about the thermodynamic quantities of the system (i.e. specific heat, energy, magnetization, etc.), and how they change in different environments. This paper will focus on magnetization; however, the other thermodynamic quantities are also useful. These quantitates heavily depend

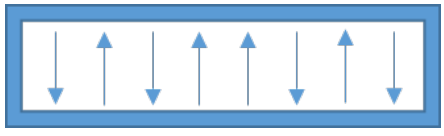

Fig. 1: 1D Ising Model with randomly assigned spins

on the interactions between neighboring spins and are functions of temperature. Thus, to maintain translational invariance and continuity, we will impose a periodic boundary condition to our model. This transforms the model into an Ising chain, which can be seen in figure 2.

The number of possible states for a system of size N is 2^N; thus, as N increases, the state space grows exponentially. A large state space makes evaluating functions like equation 2 extremely difficult. Hence, we approach the problem with a Monte Carlo method that implements the Metropolis-Hastings algorithm. The analytic solution for a 1D Ising model and the Monte Carlo sampling method will be discussed in further detail in sections 1.2 and 1.3 respectively. The results from these simulations will be compared with the analytic solutions derived by Ising in section 2. In section 3, the paper will explore uncertainty quantification and relative entropy for the 1D homogenous case. Lastly, in section 4, this paper will then present the results of two-dimensional

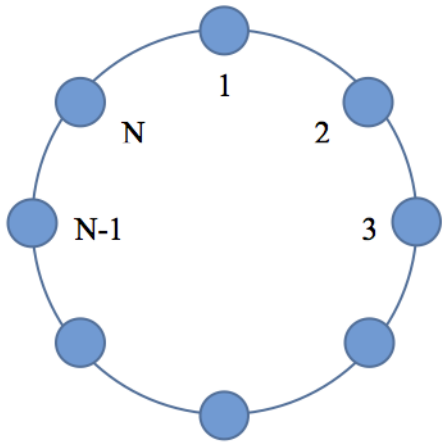

Fig. 2: 1D Ising Chain with Periodic Boundary Conditions. As the figure demonstrates, the $(N+1)^{\text{th}}$ spin is equal to the first spin.

Ising simulations.

1.2. 1D Analytic Solution

This section will follow the 1D derivation as it is written in Kerson Huang's textbook [4], for the analytic magnetization function. First, we define the energy of a specific configuration to be:

$$E_I = -\epsilon \sum_{k=1}^{N} s_k s_{k+1} - H \sum s_k \tag{1}$$

where s_k denotes the spin of the site, ϵ is the coupling constant between sites, and H is the external magnetization. Equation 1 gives rise to the system's canonical partition function

$$Q_I(H,T) = \sum_{s_1} \sum_{s_2} \cdots \sum_{s_N} e^{\beta \sum_{k=1}^{N} \epsilon s_k s_{k+1} + H s_k} \tag{2}$$

where β is the inverse temperature and each s_k independently varies between ± 1. Partition functions are useful in two main ways. First, they behave as a normalization factor for the Boltzmann distribution. To calculate the probability of a state occurring, we divide the energy value of that state by the partition function. Second, they are related to thermodynamic quantities through relationships such as the ones given in equation 3 and 4

$$f(H,T) = -kT \lim_{N\to\infty} N^{-1} Q_I(H,T) \tag{3}$$

$$M(H,T) = \frac{\partial}{\partial H} f(H,T) \tag{4}$$

where $f(H,T)$ denotes the Hemholtz free energy, and $M(H,T)$ denotes magnetization per spin. The partition function given in equation 2 above can be expressed as a product of P matrices (called transfer matrices), where P is a $2x2$ matrix whose elements are of the following form

$$\langle s|P|s'\rangle = e^{\beta \epsilon s s' + \frac{H(s_k + s_{k+1})}{2}} \tag{5}$$

where s and s' independently vary between ± 1. This gives us the following matrix P

$$P = \begin{bmatrix} e^{\beta(\epsilon+H)} & e^{-\beta(\epsilon)} \\ e^{-\beta(\epsilon)} & e^{\beta(\epsilon-H)} \end{bmatrix} \tag{6}$$

This allows the partition function to be rewritten as

$$\begin{aligned} Q_I(H,T) &= \sum_{s_1}\sum_{s_2}\dots\sum_{s_N}\langle s_1|P|s_2\rangle\langle s_2|P|s_3\rangle\dots\langle s_N|P|s_1\rangle \\ &= \sum_{s_1}\langle s_1|P|s_1\rangle \\ &= TrP^N = \lambda_+^N + \lambda_-^N \end{aligned} \tag{7}$$

where $\lambda_+^N + \lambda_-^N$ are eigenvalues. These eigenvalues are calculated to be

$$\lambda_\pm = e^{\beta\epsilon}(cosh(\beta H) \pm \sqrt{sinh^2(\beta H) + e^{-4\beta\epsilon}}) \tag{8}$$

$$\lim_{N\to\infty}\frac{1}{N}\log Q_I(H,T) = \log\lambda_+ + \log\left(1 + (\frac{\lambda_-}{\lambda_+})^N\right) = \log\lambda_+ \tag{9}$$

Using equations 3, 4, and 9 we can derive the analytic equations for free energy and magnetization.

$$\frac{1}{N}f(H,T) = -\epsilon - kT\ln cosh(\beta H) + \sqrt{sinh^2(\beta H) + e^{-4\beta\epsilon}} \tag{10}$$

$$\frac{1}{N}M(H,T) = \frac{sinh(\beta H)}{\sqrt{sinh^2(\beta H) + e^{-4\beta\epsilon}}} \tag{11}$$

Equation 11 will useful in evaluating the accuracy of our simulations.

1.3. Sampling

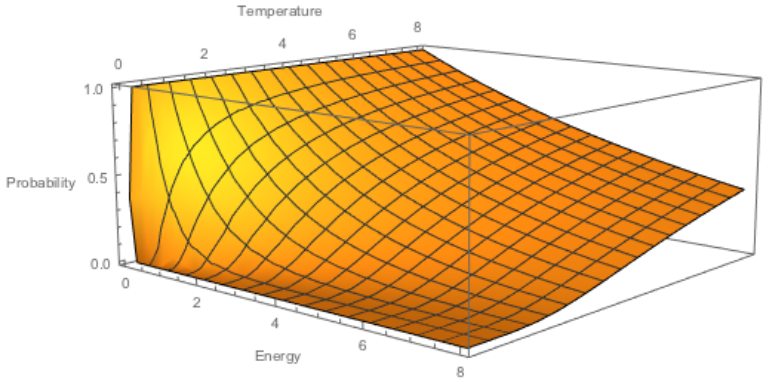

Fig. 3: Boltzmann probability distribution is shown above. As the energy of a state increases, the probability of that state occurring decreases. A similar trend can be observed with temperature. It should also be noted that temperature's effect on probability increases with energy. In particular, at low energy states the probability is only slightly influenced by energy, whereas at high energy states the probability increases with temperature.

As mentioned above, this study used a Monte Carlo simulation to model the behavior of the 1D Ising model. The initial code for the simulation was translated into Java from a MATLAB source file from [3]. Each test consisted of 10,000 Monte Carlo steps, and each Monte Carlo step consisted of N^2 Metropolis-Hastings steps. In each Metropolis step, a site in the lattice is randomly selected and the change in energy for flipping the site is calculated. If flipping the site would cause the system would move to a more energetically favorable state (lower energy states

are more favorable), then the site is flipped. If the flip would result in a less favorable state, then the flip occurs with a probability determined by the Boltzmann probability distribution

$$P(\alpha) = ce^{-E(\alpha)\beta} \tag{12}$$

$$\beta = \frac{1}{kT} \tag{13}$$

where α denotes a particular configuration, $E(\alpha)$ is the configuration's energy, β is inverse temperature, and k is the Boltzmann constant. The distribution is best visualized in figure 3. A flow chart of our tests can be seen in figure 4.

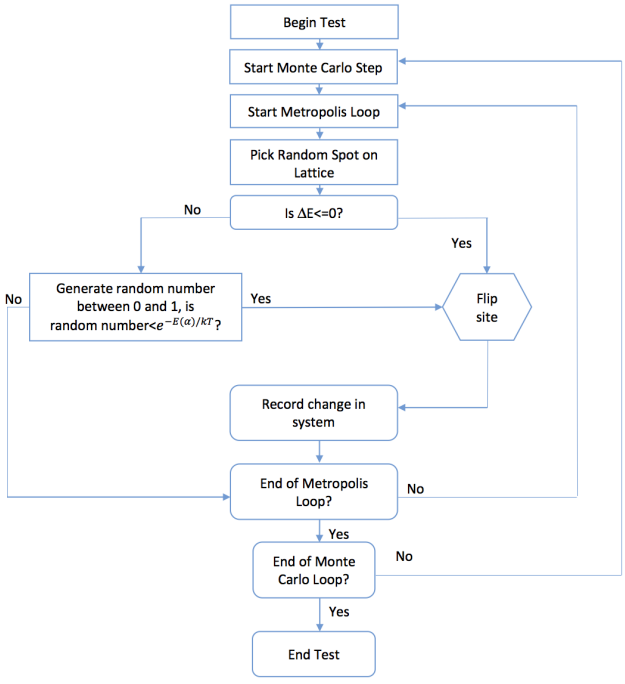

Fig. 4: The flowchart of the simulation is shown here. The simulation is composed of two nested for-loops. The outer Monte Carlo loop runs for 10,000 iterations each time, and the inner Metropolis-Hastings loops runs for N^2 iterations.

2. 1D Results

2.1. Regular 1D Ising Model

For our simulations, we tested the model at 3 different external magnetizations (H=0,1,2). The results of H=0, 1 cases are shown in figure 5 (H=2.0 was similar to H=1.0 and is thus excluded), and are compared to the magnetization values derived in equation 11. The initial lattice was created randomly with a slight bias towards positive spins. This bias was necessary because an unbiased lattice would result in a positively charged system for half the trials and a negatively charged system for the other half. Thus, when all the trials are averaged, we would falsely see an unmagnetized lattice. As expected, the H=0 case did not result in a magnetized lattice at any temperature. The H=1.0 graph shows the typical behavior of a ferromagnetic lattice. At low temperatures the lattice becomes aligned to minimize disorder and stays in that state. Hence, we see a magnetized lattice. However, as the temperature increases, the lattice sites become more

unstable and often flip even if it is energetically unfavorable. This reduces the number of aligned spins, and eventually the lattice becomes demagnetized. This phenomena is seen in figure 5b.

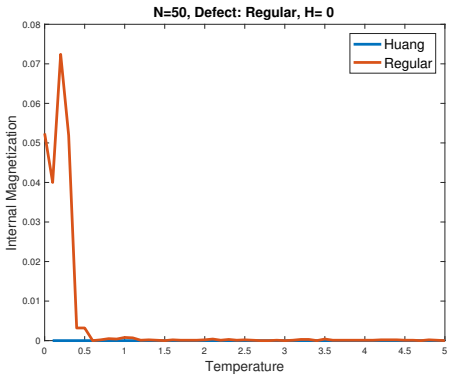

(a) Case: Regular lattice, H=0. In this test the lattice did not magnetize significantly at any temperature, which agrees with the theoretical expectation from equation 11.

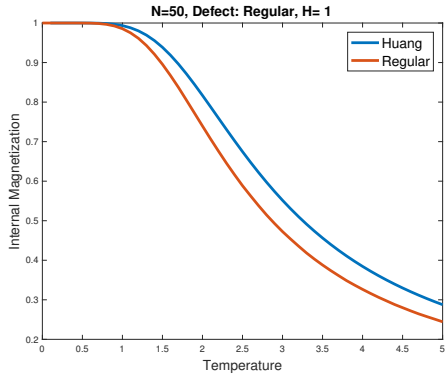

(b) Case: Regular lattice, H=1.0. In this test the lattice became magnetized at low temperatures. As temperature increased, the lattice became demagnetized. Again, the results agree with the analytic equation derived in section 1.2.

Fig. 5: Results of 1D Simulation vs. Analytic Equation

2.2. 1D Defects

Next, we will examine defective 1D Ising models. The study of defective Ising models is useful as their non-homogeneity is more applicable to the real world. We ran simulations of 2 different defects denoted 'positive' and 'split'. In the positive defect case we fixed both end sites on the lattice to have a positive spin. In the split case we fixed one end to have a fixed positive spin and the other to have a fixed negative spin. The derivation for the analytic equations for the defect cases is shown in the appendix. While the derivation for these special cases differs slightly from the homogenous case, the analytic equation remains the same as N (size of system) approaches infinity. Results of these cases can be seen in figure 6.

As seen from figure 6a above, there is a distinct difference between the computational and theoretical magnetizations for the positive defect case at H=0. This difference in magnetization can be attributed to the finite nature of the simulation. The influence of the positive fixed spin sites in a finite system of relatively small size (N=16 to N=100) is overemphasized. However, as N approaches infinity, we expect the influence of the defects to become minimized and the simulation to agree with the analytic equation. The results of H=1 are more promising as seen in figure 6b. The simulation shows that the two defective cases, while slightly shifted downward, followed the general trend of Huang's result.

3. Relative Entropy and Goal Divergence

Following the study of the 1D Ising models, we wanted to introduce an uncertainty quantification bound for the simulations we conducted. To do this, we explored a subtopic of Information Theory called relative entropy. The following discussion on relative entropy and uncertainty quantification will be heavily derived from [5]. Information Theory provides us with tools to not only construct, but also evaluate the validity of probabilistic models. Validity can be measured using a variety of metrics: Total Variation, Kullback-Leibler divergence, Relative Rnyi entropy, χ^2 divergence, Hellinger distance (the formulas defining these metrics can be found in [5]). However, as the paper goes on to show, these various metrics scale poorly with the system's size, and thus, a new metric is needed. Another paper, [2], derives this new metric, Goal-Oriented Divergence,

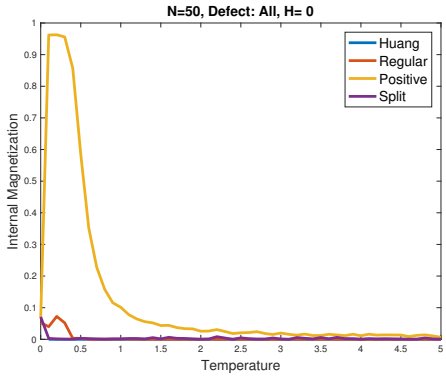

(a) Case: Defective lattice, H=0. The results of the 'positive' and 'split' defects are shown above. The positive defect case differs significantly from the expected result at low temperatures. This can be explained by the finite nature of our simulation (N=50). The relatively small lattice is heavily influenced by the fixed positive spin sites and becomes magnetized. However, as N approaches infinity, the lattice should agree with the analytic equation shown in section 1.2. This idea of exaggerated influence is further supported by the split defect case. The split case lattice does not magnetize; this can be explained as the result of the cancelation of the influences caused by the fixed positive and negative sites.

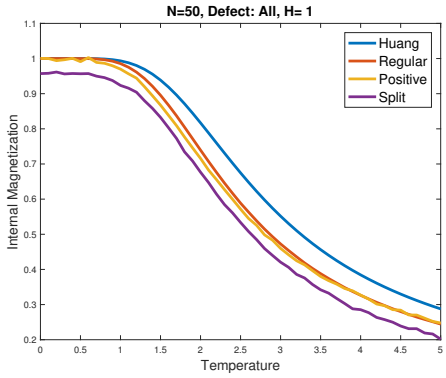

(b) Case: Defective lattice, H=1.0. In this test, the simulation results agree much more closely with the theoretical prediction.

Fig. 6: Results of 1D Defective lattice simulation vs. Analytic equation

whose upper and lower bounds are defined in equations 14 and 15

$$\Xi_+(Q||P;f) = \inf_{c>0}\{\frac{1}{c}\widetilde{\Lambda}_{P,f(c)} + \frac{1}{c}R(Q||P)\} \tag{14}$$

$$\Xi_-(Q||P;f) = \sup_{c>0}\{\frac{-1}{c}\widetilde{\Lambda}_{P,f(-c)} - \frac{1}{c}R(Q||P)\} \tag{15}$$

where Q and P represent probability distributions, f is the quantity of interest (in our case magnetization), c is a constant that will be minimized, $\widetilde{\Lambda}_{P,f(c)}$ is the cumulant generating function, and $R(Q||P)$ is the relative entropy. This Goal-Oriented Divergence is essentially a measure of how 'different' we can expect Q and P to be. It is also important to note that this is a divergence, not a distance, measure. Thus, in general, $\Xi_\pm(Q||P;f) \neq \Xi_\pm(P||Q;f)$. The final results of the relative entropy and cumulant generating functions are given in equations 16 and 17, but their derivations are shown in the appendix of [5]

$$\begin{aligned}\lim_{N\to\infty}\frac{1}{N}R(Q||P) = \log\frac{e^{\beta J}\cosh(\beta h) + \sqrt{e^{2J\beta}\sinh^2(h\beta) + e^{-2J\beta}}}{e^{\beta' J'}\cosh(\beta' h') + \sqrt{e^{2J'\beta'}\sinh^2(h'\beta') + e^{-2J'\beta'}}} \\ + (\beta' J' - \beta J)(1 - \frac{1}{\kappa_1'}\frac{2e^{-2\beta' J'}}{e^{\beta' J'}\cosh(\beta' h') + \kappa_1'}) + (\beta' h' - \beta h)\frac{1}{\kappa_1'}e^{J'\beta'}\sinh(h'\beta')\end{aligned} \tag{16}$$

$$\lim_{N\to\infty}\frac{1}{N}\widetilde{\Lambda}_{\mu_N}(c)=\log\frac{e^{\beta J}\cosh\left(\beta h+c\right)+\sqrt{e^{2J\beta}\sinh^2\left(h\beta+c\right)+e^{-2J\beta}}}{e^{\beta J}\cosh\left(\beta h\right)+\sqrt{e^{2J\beta}\sinh^2\left(h\beta\right)+e^{-2J\beta}}} \tag{17}$$

$$\kappa_1=\sqrt{e^{2J\beta}sinh^2(h\beta)+e^{-2J\beta}} \tag{18}$$

where β is the inverse temperature, h is the external magnetization, and J is the coupling constant. Figure 7 shows the Goal-Oriented divergence bounds and simulation results for a 1D model with h=0 and h=1.0. As the figure shows the simulation results are within the error margins.

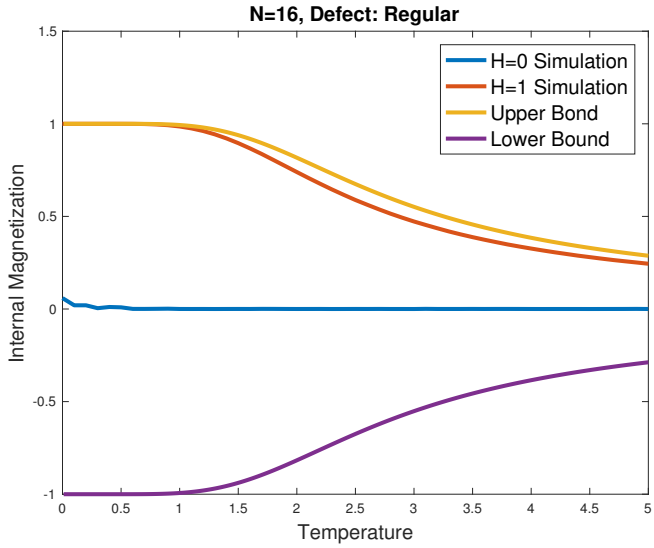

Fig. 7: Goal-Oriencted Divergence bounds for the h=0 and h=1.0 of non-defective cases. The simulation results for these cases are within the bounds predicted by the formula.

4. 2D Ising Model

Following the study of 1D Ising models, we expanded our simulations to two dimensional models. We studied a total of 6 different models (1 regular, 5 defective cases) on 4 different lattice sizes (N=16,25,50,100) for 24 total tests. The results for N=16 are shown in figures 8 and 9; however, the trends displayed in these figures were consistent for all of the lattice sizes. The first four defects we studied were similar to the 1D site defects. For first case, "Single Seed", we fixed the top left corner of the lattice to have a fixed positive spin. The second case, "Positive", we added another fixed positive spin site next to the previous one. The third case, "Dipole Seed", we changed the second fixed positive spin to a fixed negative spin. The fourth case, "Split Seed", we kept the top left corner as the fixed positive spin, but moved the fixed negative spin to the center of the lattice. All four site defects behaved relatively similar to each other and to the base case. This result suggests that the macroscopic magnetization of the lattice is immune to a small number of site defects, which seems like a reasonable finding. Following the study of fixed point defects, we chose to study a single bond defect. This defect altered the regular bond between the $(\frac{n}{2},\frac{n}{2})$ and $(\frac{n}{2}+1,\frac{n}{2}+1)$ site from J to $-10J$. The magnetization graph for the results is given in figure 9 and resembles the base case.

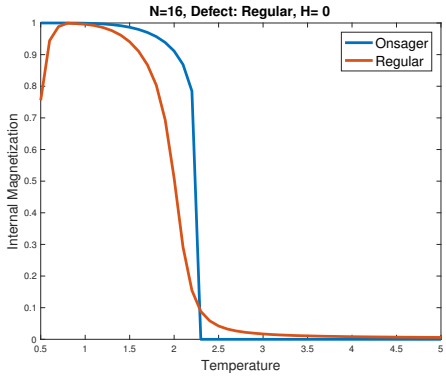

(a) Case: Non-defective lattice, H=0.

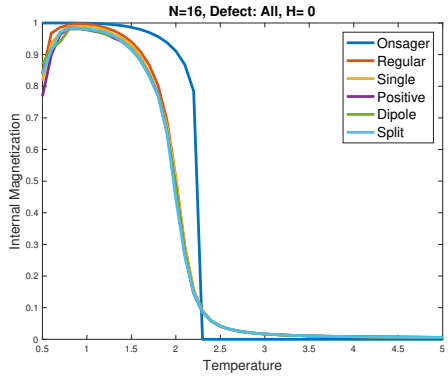

(b) Case: Non-defective lattice, H=1.0

Fig. 8: Results of 2D Simulation vs. Analytic Equation. The simulation roughly agrees with the analytic equation for most of the temperatures. However, there is a tendency for the simulated lattice to be slightly below the expected magnetization at low temperatures. The cause of this tendency requires further research. In addition, the defective lattices behave like the regular lattice meaning that a small number of fixed spin sites do not alter the lattice significantly.

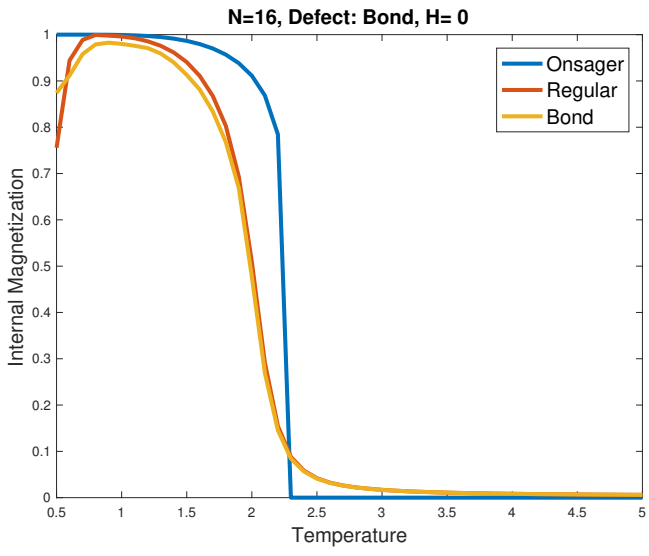

Fig. 9: Bond Defect Magnetization. The bond defect case behaved similarly to the regular case and the other defect cases.

5. Conclusions and Future Work

In general, the results from our various tests agreed with the extensive literature about Ising models. As we expected, the lattice became demagnetized as the temperature increased due to increasing instability. In addition, an external magnetization force is necessary for the 1D lattice to magnetize. We also found that single site defects neither alter the magnetic behavior of the lattice, nor create domains of similar spin. What is still left to derive are the analytic magnetization equations for the 2D defect cases, and the corresponding formulas for the Goal-Oriented divergence. Both tasks are rather involved endeavors. In addition, performing autocorrelation tests to measure how well each site is correlated to its neighbors would provide insight into the internal

behavior of the lattice.

Acknowledgements

Thank you to Dr. Dobson for the continued guidance and support throughout this project. In addition, thank you to Jie Wang and Dr. Katsoulakis for helping us with the uncertainty quantification bounds section. The initial source code for the project is from Dr.Flammia's website (professor at the University of Sydney).

References

[1] Rodney J. Baxter *Exactly Solved Models in Statistical Mechanics*, Courier Corporation, 2007.
[2] Paul Dupuis, Markos A. Katsoulakis, Yannis Pantazis, and Petr Plechc *Path-Space Information Bounds for Uncertainty Quantification and Sensitivity Analysis of Stochastic Dynamics*, SIAM/ASA Journal on Uncertainty Quantification, 2016.
[3] Steve Flammia *http://www.physics.usyd.edu.au/ sflammia/Courses/StatMech2016/advanced/4/a4.html*, Accessed Feburary.
[4] Kerson Huang *Statistical Mechanics*, John Wiley & Sons, 1963.
[5] Markos Katsoulakis, Luc Rey-Bellet, Jie Wang *Scalable Information Inequalities for Uncertainty Quantification*, Journal of Computational Physics, 2017.
[6] Jacques Kotze *Introduction to Monte Carlo methods for an Ising Model of a Ferromagnet*, conference presentation at SASNAM 2003, 2001.

Appendix

APPENDIX A: 1D Defect

As mentioned in section 2.2, we will derive the analytic equations for the 'positive' and 'split' cases for the 1D Ising model. The derivation for these equations is almost exactly the same as the regular case. Picking up from the P matrix defined in section 1.2, we have

$$P = \begin{bmatrix} e^{\beta(\epsilon+H)} & e^{-\beta(\epsilon)} \\ e^{-\beta(\epsilon)} & e^{\beta(\epsilon-H)} \end{bmatrix} \tag{19}$$

Now, we can diagonalize P so that it can be written as such:

$$P = D^{-1}AD \tag{20}$$

such that

$$D = \begin{bmatrix} v_{(1,1)} & u_{(2,1)} \\ v_{(1,2)} & u_{(2,2)} \end{bmatrix} \tag{21}$$

and

$$A = \begin{bmatrix} \lambda_1 & 0 \\ 0 & \lambda_2 \end{bmatrix} \tag{22}$$

where v and u are normalized eigenvectors whose corresponding eigenvalues are λ_1 and λ_2. For our purposes, let λ_1 denote the larger eigenvalue, and let $c_1 \dots c_8$ denote constants that are generated from multiplying $D^{-1}AD$. Thus,

$$P^N = D^{-1}A^N D = \begin{bmatrix} c_1(\lambda_1)^N + c_2(\lambda_2)^N & c_3(\lambda_1)^N + c_4(\lambda_2)^N \\ c_5(\lambda_1)^N + c_6(\lambda_2)^N & c_7(\lambda_1)^N + c_8(\lambda_2)^N \end{bmatrix} \tag{23}$$

For the positive case, we are only concerned with the $\langle +1|P|+1\rangle$ case, so we will only focus on the top left element of the matrix. As shown in equation 24, once we take the limit of the top left element as $N \to \infty$, the result becomes the largest eigenvalue (in this case λ_1), which is similar to the regular case.

$$\lim_{N\to\infty} c_1(\lambda_1)^N + c_2(\lambda_2)^N = \lambda_1 \tag{24}$$

Similarly, in the split defect case, we are only concerned about the $\langle +1|P|-1\rangle$ element or the top right corner of the matrix. This limit has the same result equation 24.

$$\lim_{N\to\infty} c_3(\lambda_1)^N + c_4(\lambda_2)^N = \lambda_1 \tag{25}$$

Thus, both the cases result in the same analytic magnetization equation as the regular case.

$$\frac{1}{N}M(H,T) = \frac{sinh(\beta H)}{\sqrt{sinh^2(\beta H) + e^{-4\beta\epsilon}}} \tag{26}$$